Nanoscale

PAPER

View Article Online
View Journal | View Issue

Cite this: *Nanoscale*, 2016, **8**, 2711

Electron beam controlled covalent attachment of small organic molecules to graphene†

Alexander Markevich,[a] Simon Kurasch,[b] Ossi Lehtinen,[b] Oliver Reimer,[c] Xinliang Feng,[d] Klaus Müllen,[d] Andrey Turchanin,[e] Andrei N. Khlobystov,[a] Ute Kaiser[b] and Elena Besley*[a]

Received 28th October 2015,
Accepted 24th December 2015

DOI: 10.1039/c5nr07539d

www.rsc.org/nanoscale

The electron beam induced functionalization of graphene through the formation of covalent bonds between free radicals of polyaromatic molecules and C=C bonds of pristine graphene surface has been explored using first principles calculations and high-resolution transmission electron microscopy. We show that the energetically strongest attachment of the radicals occurs along the armchair direction in graphene to carbon atoms residing in different graphene sub-lattices. The radicals tend to assume vertical position on graphene substrate irrespective of direction of the bonding and the initial configuration. The "standing up" molecules, covalently anchored to graphene, exhibit two types of oscillatory motion – bending and twisting – caused by the presence of acoustic phonons in graphene and dispersion attraction to the substrate. The theoretically derived mechanisms are confirmed by near atomic resolution imaging of individual perchlorocoronene ($C_{24}Cl_{12}$) molecules on graphene. Our results facilitate the understanding of controlled functionalization of graphene employing electron irradiation as well as mechanisms of attachment of impurities *via* the processing of graphene nanoelectronic devices by electron beam lithography.

Introduction

Graphene, two-dimensional sp^2-hybridizied carbon atoms arranged in a honeycomb pattern, is one of the most extensively studied materials due to its impressive range of superior mechanical, electronic, optical and transport properties. In its pristine form, graphene has been found to be a promising component in a great number of applications including touch screens, spintronic devices, fuel cells and flexible electronics.[1–5] In spite of its great application potential, pristine graphene is believed to be rather inert to chemical reactions, which weakens its competitive strength in the areas of semiconductor devices and sensors. Recently, there has been a surge of interest in functionalization of graphene using chemical reactions with organic and inorganic molecules as well as chemical modification of large areas of its surface aimed at gaining control over the band gap opening of graphene. The manipulation of a band gap by chemical doping is a desirable and powerful feature for the use of graphene in functional nanoelectronic devices.[6,7]

It is also worth noting that the purity of graphene is naturally, and very easily, affected by the environment. Organic residues, charged impurities, surface contaminants, even atmospheric oxygen, all contribute to local doping of graphene. Contaminants have an adverse effect on production and reliable synthesis of large-scale, high-quality pure graphene, which remains key to its successful applications. Adsorption of contaminants on graphene surface and unintentional doping may lead not only to its structural deformation but also to an inhomogeneous charge density and a shift in Dirac voltage.[8–12] In general, contaminant molecules act as external scattering centers and modify the properties of graphene, with the covalently attached contaminants having the strongest effect.[13–17] While smart choices of solvents and chemicals are required to limit contamination in graphene-based electronics, organic residues from fabrication are inherent in *any* graphene processing and in particular by electron beam lithography.

---

[a] *School of Chemistry, University of Nottingham, NG7 2RD Nottingham, UK. E-mail: elena.besley@nottingham.ac.uk*
[b] *Electron Microscopy Department of Material Sciences, University of Ulm, 89081 Ulm, Germany*
[c] *Faculty of Physics, University of Bielefeld, 33615 Bielefeld, Germany*
[d] *Max Planck Institute for Polymer Research, Ackermannweg 10, 55128 Mainz, Germany*
[e] *Institute of Physical Chemistry, Friedrich Schiller University Jena, Lessingstraße 10, D-07743 Jena, Germany*

† Electronic supplementary information (ESI) available: A table showing the calculated binding energies and magnetic moments for all studied molecular radicals; details of samples preparation and characterization; time series of TEM images showing transformations of a $C_{24}Cl_{12}$ molecule on graphene under electron irradiation. See DOI: 10.1039/c5nr07539d

In this paper, we explore functionalization reactions of graphene through the formation of covalent bond(s) between free radicals and C═C bonds of pristine graphene surface using first principles calculations and high-resolution transmission electron microscopy (HRTEM). Graphene displays particularly high affinity to the so-called hydrocarbon contamination[18] dominated by π–π interactions to the flat surface[19] thus making polycyclic aromatic hydrocarbons (PAHs) one of the most common organic contaminants of graphene. The hydrophobic properties and molecular sizes of PAHs affect their adsorption on graphene. The HRTEM images[20] reveal that after loading with PAHs, the potential adsorption sites of graphene can be altered during the imaging process. However, the detailed HRTEM study of the adsorption behaviors of PAHs on graphene at a molecular level is hindered by electron irradiation damage during imaging. The imaging electron beam (e-beam) breaks readily the C–H bond and destroys individual small PAH molecules over time. The prime example is a coronene molecule, which has been observed to decompose very fast in the HRTEM at energies of 80–120 keV.[21] A simple and elegant solution to increase stability of organic molecules under the e-beam has been proposed recently[22] through substitution of protium isotope of hydrogen for deuterium. Isotopic substitution has no effect on the molecular structure but increases the atomic weight of the hydrogen atoms by 100%, which drastically improves the stability of organic molecules (or crystals) in the HRTEM, thus allowing imaging of individual species. Another effective approach to enhance the stability of organic molecules in HRTEM is halogenation, although substitution of hydrogen with halogens alters the original chemical properties of the molecules. It has been observed[23,24] that halogenated substituents of benzene, benzoquinone and phthalocyanine, where all hydrogen atoms are replaced for much heavier atoms, exhibit greater durability against electron irradiation. A HRTEM study of perchlorocoronene, $C_{24}Cl_{12}$, suggests its high stability against the e-beam.[25] The damaging mechanisms for disintegration of crystalline $C_{24}Cl_{12}$ during electron radiation have been previously studied using HRTEM, electron diffraction, and electron energy-loss spectroscopy.[26]

It is well known that hydrocarbons adsorbed on graphene diffuse along its surface towards the edge of the irradiated area or towards large structural defects (typically extended vacancy lines or holes) where they are immobilized by forming covalent bonds with carbon atoms at the edge of the defected area.[18] An alternative example of chemical functionalization of the graphene surface is an addition of organic free radicals to sp^2 carbon atoms of pristine graphene. The free radical addition method has been recently tested[27] to achieve the reaction of benzoyl peroxide with graphene sheets, which was induced photochemically (using focused Ar-ion laser beam). The attachment of the phenyl groups was directly indicated by the appearance of a strong D-band at 1343 cm^{-1} in the Raman spectrum, which is due to the formation of sp^3 carbon atoms in the basal plane of graphene by covalent attachment of phenyl groups. In this case, the covalent addition of phenyl groups to graphene led to a significant decrease in conductivity due to disruption of the aromatic system *via* transformation of carbon atoms from sp^2 to sp^3 hybridization.

In the present work we demonstrate the creation of free radicals of small organic molecules and their covalent chemical attachment to graphene during HRTEM imaging. The radicals strongly anchored to graphene are amenable to HRTEM imaging, unlike highly mobile physisorbed molecules. Since imaging of PAHs on graphene by HRTEM is not currently possible, we have deposited perchlorocoronene, $C_{24}Cl_{12}$, molecules on graphene and observed in HRTEM structural transformations induced by the e-beam in real time with near-atomic resolution. We find that perchlorocoronene radicals are preferably aligned along the armchair direction in graphene, which is consistent with our theoretical predictions for PAHs. Time series of HRTEM imaging clearly demonstrate switching between the vertical ("stand up") and near horizontal ("lie down") positions of perchlorocoronene radical. This can be understood by the interplay between the strain in covalent bonds formed between the radicals and graphene and the van der Waals attraction, as demonstrated by classical molecular dynamics (MD) simulations. The comparison between theoretically predicted behavior of PAH radicals anchored to graphene and stable halogenated PAH radicals on graphene observed in HRTEM reveals common dynamic behavior and chemical transformations of small radicals on graphene and enables capturing the atomistic mechanisms of the chemical bond formation.

Results and discussion

Aromatic hydrocarbons, ubiquitous impurities present during the growth and processing of graphene, undergo rapid damage under the e-beam of a HRTEM during the imaging process, which primarily starts at the C–H bond as the extremely light hydrogen atoms are rapidly removed at the energies of e-beam of 60–80 keV, which are typically used for imaging graphene in high resolution. This results in the formation of PAH free radicals. The structure and energetic properties of most commonly occurring PAH radicals, namely, benzene, C_6H_6, naphthalene, $C_{10}H_8$, anthracene, $C_{14}H_{10}$, phenanthracene, $C_{14}H_{10}$, and coronene, $C_{24}H_{12}$, adsorbed on graphene, both in chemisorption and physisorption, have been studied using density functional theory (DFT) with PBE form of the exchange–correlation functional[28] and Grimme dispersion corrections.[29] The counterpoise corrected[30] values of the binding energy calculated as the difference in the total energy of isolated and interacting fragments are shown in Table 1 for the molecules and their radicals physisorbed on graphene in the AB stacking configuration. The experimental values of the binding energy determined with the use of the Redhead analysis[31] of the thermal desorption spectra have been reported to be E_b = (0.50 ± 0.08) eV for benzene, E_b = (0.8 ± 0.1) eV for naphthalene, and E_b = (1.3 ± 0.2) eV for coronene molecule.[32] The Falconer–Madix analysis[33] of the same thermal desorption spectra produced the values of E_b = (0.90 ± 0.07) eV for

Table 1 The PBE + D binding energies for several polycyclic aromatic hydrocarbons and their radicals physisorbed on graphene

Molecule	C_6H_6	$C_{10}H_8$	$C_{14}H_{10}$	$C_{14}H_{10}$	$C_{24}H_{12}$
E_b, eV	0.38	0.60	0.81	0.82	1.33
Radical	C_6H_5	$C_{10}H_6$	$C_{14}H_6$	$C_{14}H_7$	—
E_b, eV	0.36	0.56	0.74	0.76	—

naphthalene and $E_b = (1.5 \pm 0.1)$ eV for coronene molecule. These experimental values are slightly higher than the values reported in the present work. However, the calculated binding energies agree well with previously published theoretical data for physisorption energies, which vary in the range of 0.34 eV–0.66 eV for benzene molecule,[19,34,35] 0.59 eV–0.76 eV for naphthalene and 1.29 eV–1.73 eV for coronene[19,35] depending on the method of treatment of van der Waals forces and basis set size used in the calculations. As shown in Table 1 the binding energies of physisorbed radicals were found to be only slightly smaller than the binding energies of the corresponding molecules suggesting that there is no significant direct interaction between the under-coordinated C atoms of a radical and graphene. This indicates that covalent bonds between the radicals and pristine graphene are not likely to form instantaneously.

Formation of covalent bonds between free radicals and graphene can be either thermodynamically driven or promoted by collisions with high-energy electrons of the imaging beam. The outcome of functionalization depends on the structure of a newly formed reactive carbon edge (armchair or zigzag) and the relative position of the radical edge with respect to the graphene substrate. For the smallest member of the studied family – benzene molecule – four possible chemisorption configurations on graphene are considered, as depicted in Fig. 1a–d, which are labeled to distinguish between different bonding sites within a hexagon in the graphene lattice. Mono-radical of benzene C_6H_5 (phenyl radical), shown in Fig. 1a, exhibits the binding energy of $E_b = 0.99$ eV and the magnetic moment of $M = 1\mu_B$. In contrast, benzene bi-radical demonstrates different bonding modes on graphene, which are denoted as the 1,2-bonding (Fig. 1b), the 1,3-bonding (Fig. 1c), and the 1,4-bonding (Fig. 1d) positions. In the 1,2- and 1,4-bonding positions, the bi-radical is attached to graphene carbon atoms residing in different sub-lattices (shown in Fig. 1e in different color: yellow and blue), and it is aligned along the armchair direction in graphene. The binding energies of the 1,2- and 1,4-bonding positions are found to be very similar, namely $E_b = 1.15$ eV for the 1,2-bonding and $E_b = 1.13$ eV for the 1,4-bonding, and both configurations have zero magnetic moment. In a metastable 1,3-bonding position, the bi-radical of benzene is bound to carbon atoms in the same graphene sub-lattice, and it is aligned along the zigzag direction in graphene. The calculated binding energy for the 1,3-bonding position is only $E_b = 0.29$ eV, which is even smaller than a typical physisorption binding energy for

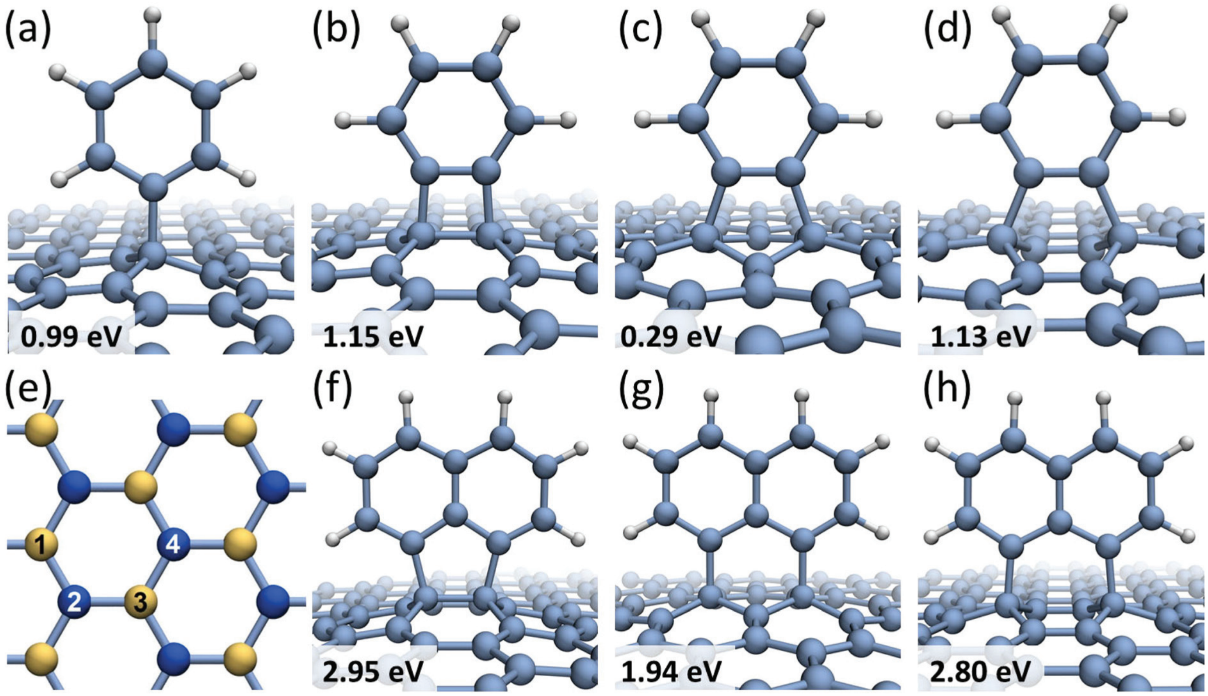

Fig. 1 Chemisorption sites for benzene and naphthalene radicals on graphene with the calculated binding energies: (a) the bonding position of phenyl radical; (b) the 1,2-bonding; (c) the 1,3-bonding; (d) the 1,4-bonding positions of benzene bi-radical; (e) a diagram showing labeling of carbon atoms in graphene lattice; atoms corresponding to different graphene sub-lattices are shown in different color (yellow and blue); (f) the 1,2-bonding; (g) the 1,3-bonding; (h) the 1,4-bonding positions of the 1,8-$C_{10}H_6$ bi-radical.

benzene radicals. The magnetic moment $M = 2\mu_B$ of the 1,3-bonding position indicates that the lack of stability is related to the fact that the 1,3-bonding to graphene leads to a structure with open electronic shell (two topologically isolated unpaired electrons which cannot recombine). As a result the 1,2- and 1,4-bonding structures are both much more stable than the 1,3-bonding structure, even though they are more sterically strained. The lengths of the C–C bonds formed between the radicals and graphene vary between 1.54 Å for the case of 1,2-bonding of the C_6H_4 radical (Fig. 1b) and 1.59 Å for the C_6H_5 radical (Fig. 1a) indicating that in all cases chemical bonds between the radicals and graphene are formed. The table showing the calculated binding energies and magnetic moments for all studied radicals can be found in ESI (Table S1†).

Similar chemisorption behavior has been predicted for the 1,8-$C_{10}H_6$ bi-radical of naphthalene molecule. When the 1,8-$C_{10}H_6$ radical is bound to graphene carbon atoms in different sub-lattices (shown in Fig. 1f and h), the corresponding binding energies are very similar: $E_b = 2.95$ eV for the 1,2-bonding position and $E_b = 2.80$ eV for the 1,4-bonding position. In the 1,3-bonding position (Fig. 1g), the bi-radical 1,8-$C_{10}H_6$ is bound to carbon atoms in the same graphene sub-lattice showing a significantly lower binding energy of $E_b = 1.94$ eV. A general trend has been observed where benzene and naphthalene bi-radicals chemisorbed on graphene along the armchair direction have the total magnetic moment of $M = 0$, while in the case of chemisorption along the zigzag direction $M = 2\mu_B$. The same conclusions have been previously reached for chemisorption of atomic hydrogen on graphene layer[36,37] showing that if a pair of hydrogen atoms are bound to different graphene sub-lattices the total magnetic moment of the system is zero. However, if all hydrogen atoms are bound to the same graphene sub-lattice the magnetic moment of the system is equal to the number of covalent bonds formed.

Larger molecules form more complicated chemisorption patterns on graphene but they follow similar structural and energetic trends. For example, anthracene tri-radical, 1,8,9-$C_{14}H_7$, tends to align along the 1,4-bonding armchair direction in graphene (Fig. 2a) with the binding energy of $E_b = 4.46$ eV, which is about 1.5 eV more favorable than chemisorption along the 1,3-bonding zigzag direction (Fig. 2b). Fig. 2c and d show phenanthrene tetra-radical, 3,4,5,6-$C_{14}H_6$, aligned along the 1,2- and 1,4-bonding armchair direction in graphene. In the alignment along the 1,4-bonding armchair direction a significant deformation of graphene substrate layer occurs, however, this configuration remains energetically more favorable than the 1,2-bonding case. Regardless of the radical structure, all chemisorbed molecules are preferably bound to graphene carbon atoms residing in different sub-lattices and aligned along the armchair direction in graphene. This result agrees with a general conclusion[38] that chemisorption of atoms as well as functional groups on two different graphene sub-lattices is energetically more favorable than chemisorption on the same sub-lattice.

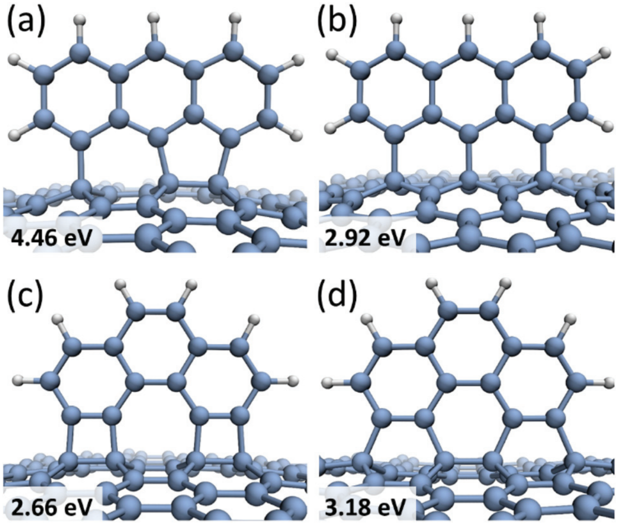

Fig. 2 Chemisorption sites for anthracene and phenanthrene radicals on graphene with the calculated binding energies: 1,8,9-$C_{14}H_7$ tri-radical is aligned along (a) the 1,4-bonding armchair; (b) the 1,3-bonding zigzag direction; the 3,4,5,6-$C_{14}H_6$, $C_{14}H_6$ tetra-radical is aligned along (c) the 1,2-bonding armchair; (d) the 1,4-bonding armchair direction.

The dynamical behaviour of chemisorbed PAH radicals on graphene substrate has been studied using classical molecular dynamics with the AIREBO[39] potential. The $C_{24}H_{10}$ radical of coronene molecule has been modelled in the 1,2- and 1,4-bonding configurations. Two different initial geometries corresponding to the chemisorbed molecule either lying or standing on graphene substrate have been considered. The size of the considered molecule implies that the dispersion attraction to the substrate will make a significant contribution to the total binding energy. The physisorption energies calculated with the AIREBO potential were found to be $E_b = 0.42$ eV for C_6H_6, $E_b = 1.41$ eV for $C_{24}H_{12}$ and $E_b = 2.97$ eV for $C_{54}H_{18}$, in a good agreement with theoretical (DFT) and experimental results (see Table 1 and the accompanying text) thus suggesting that the AIREBO potential provides a realistic description of dispersion interactions. The MD simulations have shown that the $C_{24}H_{10}$ radical tends to assume vertical position on the graphene substrate irrespective of bonding direction and initial configuration. The "standing up" molecule exhibits two types of oscillating motion – bending (Fig. 3a) and twisting (Fig. 3b) – caused by the presence of acoustic phonons in graphene.

A very different behaviour has been observed for the larger $C_{54}H_{15}$ radical in the 1,4-bonding configuration. If the chemisorbed radical is initially lying on the graphene surface it remains in the same configuration for the whole time of the MD simulation (Fig. 3c). In this case, the binding energy due to the dispersion interactions between the radical and graphene is higher than the strain energy caused by the bending of sp^2 carbon bonds. However, if the initial configuration is a standing radical it does not lie down during simulation and the oscillations of the molecule are less

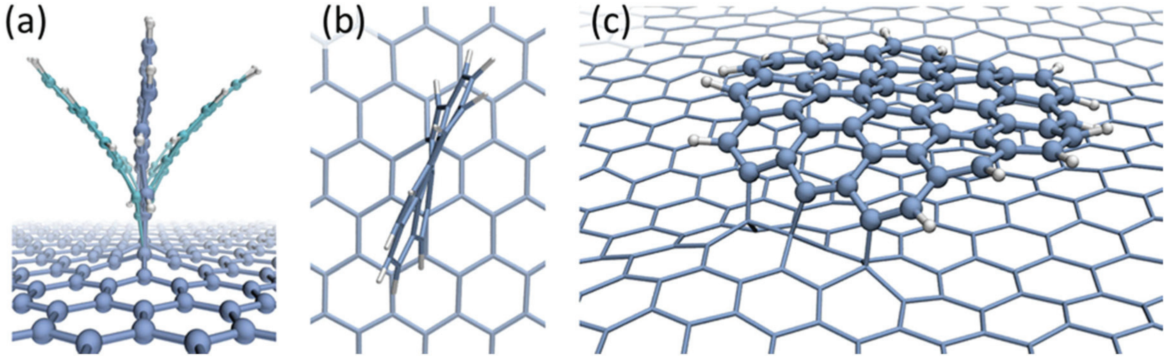

Fig. 3 Snapshots of the classical MD simulations, using AIREBO potential, showing the bending oscillatory motion of a $C_{24}H_{10}$ radical chemisorbed on graphene (a) and twisting oscillations (b); (c) a snapshot taken after 5 ns of a larger $C_{54}H_{15}$ radical chemisorbed on graphene shows that, although three covalent bonds are formed with graphene, the dispersion attraction to graphene is higher than the strain energy caused by the bending of the sp^2 carbon bonds, which causes the molecule to lie flat on graphene.

pronounced than in the case of the $C_{24}H_{10}$ radical. Stabilization of the radical in this configuration can be explained by the fact that dispersion interactions are significantly reduced compared to the case of the lying molecule and contribute only 0.4 eV to the binding energy. Formation of three covalent bonds also makes the radical more stable with regards to the oscillations compared to the chemisorbed $C_{24}H_{10}$ radical in which only two covalent bonds are formed.

It is not possible to observe directly the dynamic behavior and chemical transformations of standard PAH molecules on graphene due to the rapid onset of knock-on damage caused by the fast electrons of the e-beam during HRTEM imaging.[22] The structure of PAH molecule would need to be modified to prolong its lifetime under the e-beam exposure and to slow down the dynamics to the timescale of HRTEM imaging (*e.g.* few seconds). To achieve this, we have substituted all hydrogen atoms in coronene with chlorine atoms to form a perchlorocoronene molecule ($C_{24}Cl_{12}$) that exhibits a greater stability against electron irradiation. $C_{24}Cl_{12}$ molecules were then deposited onto graphene sheets suspended on HRTEM grids *via* physical vapor deposition at ultra-high vacuum conditions (see ESI† for details). The X-ray photoelectron spectroscopy (XPS) characterization of samples prepared at similar conditions on highly oriented pyrolytic graphite substrates demonstrates the adsorption of $C_{24}Cl_{12}$ molecules by appearance of the characteristic Cl 2s and Cl $2p_{3/2,1/2}$ peaks (see ESI†). The estimated coverage corresponds to ~1% of a monolayer. If the mechanism of chemical bond formation to graphene is similar for small hydrogenated and halogenated aromatic molecules, it is expected that once two or more chemical bonds are formed between graphene and radicals (produced from $C_{24}Cl_{12}$ damaged by the e-beam), these molecules can also rotate into a vertical position and align along the preferential armchair direction, as theoretically predicted for PAHs.

The higher stability of $C_{24}Cl_{12}$ molecule in the e-beam enabled experimental investigation of the predicted mechanisms by aberration-corrected HRTEM imaging. The heavier chlorine atoms at the molecular edge produce a stronger contrast compared to lighter C atoms in the center, so the molecules are expected to have a ring-like appearance in HRTEM images as predicted by image simulation shown in Fig. 4b. Areas of graphene as large as tens to hundreds of nm in diameter were observed, which were free from contamination, similar to the case of imaging graphene with no deposition treatment but after pre-imaging cleaning.[40]

Additionally, a large number of circles of dark contrast were observed on the otherwise clean area of graphene, as marked by the arrows in Fig. 4d. At higher magnification most of these features appeared to be ring-like structures of about 1 nm in diameter as shown in Fig. 4c and e. The shape and size of the observed structures and experimental conditions of the samples preparation indicate that the rings of dark contrast correspond to the 2D projection of the deposited $C_{24}Cl_{12}$ molecules. The molecules undergo a constant motion on the graphene surface (Fig. 4e) caused by thermal effects and electron irradiation so that the individual chlorine atoms cannot be resolved.

It has been observed that many of the adsorbed molecules occasionally undergo a reversible transformation between circular and linear projections. An example of such transformation is shown as a time series of HRTEM images in Fig. 5a. The time between the molecular transformations varies from few to hundred seconds at the dose rates used in experiment that range from 2×10^6 e nm^{-2} s^{-1} to 13×10^6 e nm^{-2} s^{-1}. Often, just before the transformation to the linear projection, the molecule exhibits a crescent-like shape with diminishing contrast at one edge indicating the loss of Cl atoms and formation of a molecular radical. We suggest that the e-beam damages the initial structure of the molecule and promotes formation of covalent bonds between the radical and the graphene substrate, which induces the rotation of the radical by 90° with respect to the graphene plane, as theoretically predicted for PAHs. In such configuration the projection of the radical has nearly a linear shape. The reversible switching between two configurations suggests that under the e-beam irradiation conditions both formation and breaking of covalent bonds between the molecular radicals and graphene occurs.

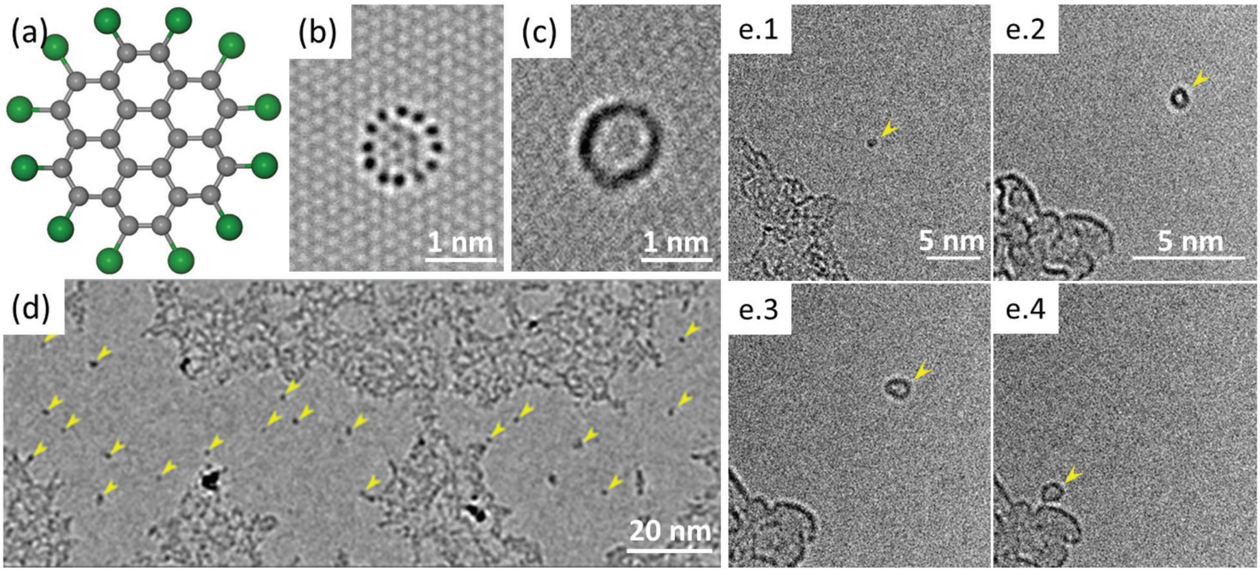

Fig. 4 $C_{24}Cl_{12}$ molecules deposited on graphene as observed by HRTEM: (a) schematic representation of the atomic structure of a $C_{24}Cl_{12}$ molecule; (b) a simulated TEM image of a $C_{24}Cl_{12}$ molecule on graphene; (c) an experimental high-magnification image of a $C_{24}Cl_{12}$ molecule on graphene (individual chlorine atoms cannot be resolved due to the high mobility of molecules on graphene); (d) overview of the sample, showing clean contamination-free areas of graphene with deposited $C_{24}Cl_{12}$ molecules observed as circles of dark contrast marked by the arrows; (e) series of HRTEM images of a single $C_{24}Cl_{12}$ molecule on graphene.

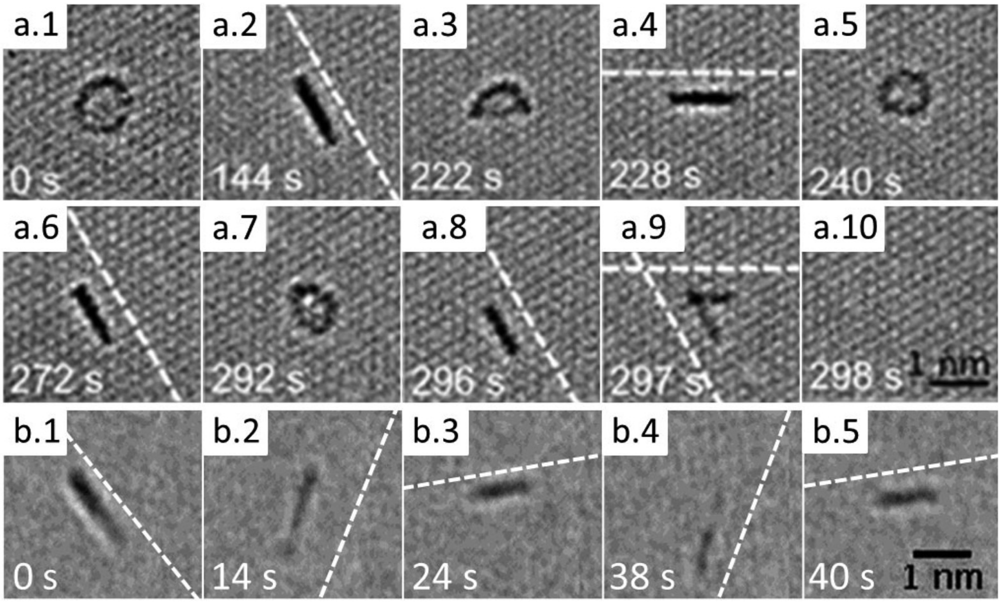

Fig. 5 Time series of HRTEM images showing (a.1–a.10) a reversible transformation between circular and linear projections of the $C_{24}Cl_{12}$ molecule on graphene; (b.1–b.5) series shows liner projection of the standing up molecule switching its orientation to match different armchair directions of graphene. The dashed lines in (a) and (b) denote the armchair direction of graphene nearest to the $C_{24}Cl_{12}$ orientation.

The molecules, when covalently attached to graphene, show remarkably consistent behaviour in terms of their orientation relative to the substrate. In full agreement with the computational predictions (both for the dynamics and stability), the molecules align along the armchair direction of graphene with no observed exceptions in our experiment. The sequences of images in Fig. 5 have the nearest armchair direction of graphene marked by the dashed lines whenever the molecule is in the 'stand-up' position. We note that the structure of the reactive edge and the binding configuration of the radicals on graphene cannot be determined from the TEM images. However, the fact "standing up" radicals are strictly aligned along the armchair direction of graphene and are stable in this configuration for extended period of time suggests that at least two covalent bonds have to be formed between the radical and graphene to promote rotation of the radical into the vertical position. Closer examination indicates that the size of the molecules tend to get smaller during imaging indicating gradual fragmentation and removal of atoms by the electron beam. Eventually the molecules are getting detached from the substrate, and either re-attach at, *e.g.*, nearby contamination, or disappear completely.

The sharp line observed in TEM images for the "stand up" state of a radical of the $C_{24}Cl_{12}$ molecule suggests that no significant oscillations of the radical occur. This is in contrast with the strong oscillating motion predicted by MD simulations for the $C_{24}H_{10}$ radical chemisorbed on graphene (see Fig. 3). It should be noted, however, that in the case of the $C_{24}Cl_{12}$ molecule the chlorine atoms constitute about 75% of the molecular mass. Therefore, the heavy edge of the molecule will strongly suppress the oscillatory motion of the lighter C skeleton caused by the presence of phonons in graphene.

Conclusions

In this work we have presented the combined theoretical and experimental investigation of the chemisorption of small aromatic molecules on pristine graphene. The results of DFT calculations show that radicals of small polyaromatic hydrocarbons chemisorbed on graphene tend to assume vertical orientation with respect to the graphene plane, and they are preferably aligned along the armchair direction of graphene regardless of the structure of the reactive edge of the radical. The TEM images of individual perchlorocoronene ($C_{24}Cl_{12}$) molecules on graphene reveal that these molecules undergo reversible transformations between the ring- and line-like structures. It suggests that the electron beam of TEM promotes formation of free radicals of the $C_{24}Cl_{12}$ molecules and their covalent attachment to the graphene substrate. The chemisorbed radicals also assume the vertical position with respect to graphene, which in TEM images appear as a line-like structure. In agreement with the computational predictions, the molecules in their 'line' state are always aligned along the armchair direction of graphene. Experimental TEM observations of dynamics of PCC molecules on graphene represent a striking example of a real-time imaging of molecular transformations with near-atomic resolution. Our results facilitate the deeper understanding of controlled functionalization of graphene employing electron irradiation and effects of impurities in graphene-based devices produced by electron beam lithography.

Methods

Simulations

PAHs adsorbed on graphene (both chemisorption and physisorption) have been studied using density functional theory (DFT) with PBE form of the exchange–correlation functional[28] and Grimme dispersion corrections,[29] as implemented in the AIMPRO code.[41] The core electron levels were treated within the Hartwigsen–Goedecker–Hutter (HGH) pseudopotentials scheme.[42] Kohn–Sham spin-polarised valence orbitals were represented by a set of atom centered s-, p-, and d-like Gaussian functions. Matrix elements of the Hamiltonian are determined using a plane wave expansion of the density and Kohn–Sham potential with a cut-off of 300 a.u. All structures were studied with periodic boundary conditions. Graphene substrate was represented by the hexagonal unit cell containing 128 carbon atoms. The Brillouin zone was sampled within the Monkhorst–Pack scheme[43] using a $(6 \times 6 \times 1)$ *k*-points grid. Optimization of the atomic positions was performed using a conjugate-gradient algorithm until the maximum force on any atom is less than 0.01 eV $Å^{-1}$.

The dynamic behaviour of the $C_{24}H_{10}$ and $C_{54}H_{15}$ radicals covalently bonded to graphene substrate has been investigated using classical MD calculations with the AIREBO potential.[39] The calculations have been carried out using LAMMPS molecular dynamics simulator.[44] The graphene layer has been represented with 680 carbon atoms and periodic boundary conditions have been employed. All structures have been initially optimized using the conjugate gradient energy minimization scheme and then equilibrated at temperature 300 K over 10 ns. The dynamic behavior of the radicals was studied in the subsequent NVE simulation for another 10 ns.

The image simulations were conducted with the QSTEM software[45] using a spherical aberration value of 20 μm, focal spread of 6 nm and Scherzer focus. The value of the electron dose was taken to be 10^7 e nm^{-2}. The experimentally measured modulation transfer function (MTF) of a CCD camera[46] at an 80 kV accelerating voltage was then applied to obtain an accurate signal to noise ratio.

Experiment

Graphene was grown on 25 μm thin copper foils (99.8%, Alfa Aesar GmbH & Co KG, Karlsruhe) using low-pressure chemical vapour deposition.[47,48] $C_{24}Cl_{12}$ powder was introduced in a Knudsen cell (Kentax Evaporator TCE-BSC), put into ultra-high vacuum and was baked out over night at 473 K. The temperature was then further increased to 523 K and after 30 min of thermal equilibration the compound was evaporated for 30 minutes onto graphene. A detailed description of the preparation of graphene samples and $C_{24}Cl_{12}$ powder can be found in ESI.†

The samples were characterized by aberration-corrected high-resolution transmission electron microscopy using an FEI Titan 80–300 microscope, equipped with an image-side spherical aberration corrector. The microscope was operated at 80 kV, and the extraction voltage of the field emission gun was set to 2 kV to reduce the energy spread of the electron beam. The spherical aberration coefficient was tuned to <20 μm and the imaging was conducted at under focus resulting in atoms appearing as dark spots in the images. The electron dose rate was $(2–13) \times 10^6$ e nm^{-2} s^{-1}.

Author contributions

AM and EB produced static and dynamic chemical calculations elucidating the mechanisms of the electron beam assisted attachment of molecules to graphene; SK and OL performed AC-HRTEM imaging on graphene and image analysis; OR prepared the samples of perchlorocoronene deposited on graphene and characterized them by XPS; XF and KM synthesised perchlorocoronene used for graphene samples; AT conceived experiments on the AC-HRTEM imaging of perchlorocoronene on graphene, supervised preparation and XPS characterization of the samples and contributed to interpretation of the AC-HRTEM data; UK conceived experiments on the AC-HRTEM imaging of perchlorocoronene on graphene, supervised the AC-HRTEM work and contributed to interpretation of the results; ANK carried out initial HRTEM imaging and contributed to interpretation of the results; AM, AT, UK, ANK and EB co-wrote the manuscript.

Acknowledgements

EB and ANK acknowledge ERC Consolidator Grants and EPSRC for financial support. AM and EB are grateful to the High Performance Computing (HPC) Facility at the University of Nottingham for providing computational time. AT, OL, UK and XF acknowledge support *via* "Graphene Flagship" and DFG SPP "Graphene". UK, SK, OL acknowledge the DFG and the Ministry of Science, Research and the Arts (MWK) of Baden-Wuerttemberg in the frame of the SALVE (Sub Angstrom Low-Voltage Electron microscopy) project. AT and OR acknowledge the Heisenberg Programme and the EMRP project "GraphOhm".

References

1 A. Reina, X. Jia, J. Ho, D. Nezich, H. Son, V. Bulovic, M. S. Dresselhaus and K. Jing, *Nano Lett.*, 2009, **9**, 30–35.
2 B. R. Van Noorden, *Nature*, 2011, **469**, 14–16.
3 V. Chandra, J. Park, Y. Chun, J. W. Lee, I. C. Hwang and K. S. Kim, *ACS Nano*, 2010, **4**, 3979–3986.
4 S. Huh, J. Park, K. S. Kim, B. H. Hong and S. Bin Kim, *ACS Nano*, 2011, **5**, 3639–3644.
5 A. C. Ferrari, F. Bonaccorso, V. Fal'ko, K. S. Novoselov, S. Roche, P. Boggild, S. Borini, F. H. L. Koppens, V. Palermo, N. Pugno, J. A. Garrido, R. Sordan, A. Bianco, L. Ballerini, M. Prato, E. Lidorikis, J. Kivioja, C. Marinelli, T. Ryhanen, A. Morpurgo, J. N. Coleman, V. Nicolosi, L. Colombo, A. Fert, M. Garcia-Hernandez, A. Bachtold, G. F. Schneider, F. Guinea, C. Dekker, M. Barbone, Z. Sun, C. Galiotis, A. N. Grigorenko, G. Konstantatos, A. Kis, M. Katsnelson, L. Vandersypen, A. Loiseau, V. Morandi, D. Neumaier, E. Treossi, V. Pellegrini, M. Polini, A. Tredicucci, G. M. Williams, B. Hee Hong, J.-H. Ahn, J. Min Kim, H. Zirath, B. J. van Wees, H. van der Zant, L. Occhipinti, A. Di Matteo, I. A. Kinloch, T. Seyller, E. Quesnel, X. Feng, K. Teo, N. Rupesinghe, P. Hakonen, S. R. T. Neil, Q. Tannock, T. Lofwander and J. Kinaret, *Nanoscale*, 2015, **7**, 4598–4810.
6 J. Park, W. H. Lee, S. Huh, S. H. Sim, S. Bin Kim, K. Cho, B. H. Hong and K. S. Kim, *J. Phys. Chem. Lett.*, 2011, **2**, 841–845.
7 J. Park, S. B. Jo, Y. J. Yu, Y. Kim, J. W. Yang, W. H. Lee, H. H. Kim, B. H. Hong, P. Kim, K. Cho and K. S. Kim, *Adv. Mater.*, 2012, **24**, 407–411.
8 S. Adam, E. H. Hwang, V. M. Galitski and S. Das Sarma, *Proc. Natl. Acad. Sci. U. S. A.*, 2007, **104**, 18392–18397.
9 J. Martin, N. Akerman, G. Ulbricht, T. Lohmann, J. H. Smet, K. von Klitzing and A. Yacoby, *Nat. Phys.*, 2008, **4**, 144–148.
10 E.-A. Kim and A. H. Castro Neto, *EPL*, 2008, **84**, 57007.
11 J.-H. Chen, C. Jang, S. Adam, M. S. Fuhrer, E. D. Williams and M. Ishigami, *Nat. Phys.*, 2008, **4**, 377–381.
12 Y. Zhang, V. W. Brar, C. Girit, A. Zettl and M. F. Crommie, *Nat. Phys.*, 2009, **5**, 722–726.
13 X. Du, I. Skachko, A. Barker and E. Y. Andrei, *Nat. Nanotechnol.*, 2008, **3**, 491–495.
14 Y. Dan, Y. Lu, N. J. Kybert, Z. Luo and A. T. C. Johnson, *Nano Lett.*, 2009, **9**, 1472–1475.
15 F. Chen, J. Xia, D. K. Ferry and N. Tao, *Nano Lett.*, 2009, **9**, 2571–2574.
16 M. Ishigami, J. H. Chen, W. G. Cullen, M. S. Fuhrer and E. D. Williams, *Nano Lett.*, 2007, **7**, 1643–1648.
17 Z. Cheng, Q. Zhou, C. Wang, Q. Li, C. Wang and Y. Fang, *Nano Lett.*, 2011, **11**, 767–771.
18 R. F. Egerton, P. Li and M. Malac, *Micron*, 2004, **35**, 399–409.
19 O. V. Ershova, T. C. Lillestolen and E. Bichoutskaia, *Phys. Chem. Chem. Phys.*, 2010, **12**, 6483.
20 J. Wang, Z. Chen and B. Chen, *Environ. Sci. Technol.*, 2014, **48**, 4817–4825.
21 B. Botka, M. E. Füstös, H. M. Tõháti, K. Németh, G. Klupp, Z. Szekrényes, D. Kocsis, M. Utczás, E. Székely, T. Váczi, G. Tarczay, R. Hackl, T. W. Chamberlain, A. N. Khlobystov and K. Kamarás, *Small*, 2014, **10**, 1369–1378.
22 T. W. Chamberlain, J. Biskupek, S. T. Skowron, P. A. Bayliss, E. Bichoutskaia, U. Kaiser and A. N. Khlobystov, *Small*, 2015, **11**, 622–629.
23 M. Koshino, H. Kurata and S. Isoda, *Microsc. Microanal.*, 2007, **13**, 96–107.
24 T. Kobayashi and K. Reimwe, *Bull. Inst. Chem. Res., Kyoto Univ.*, 1975, **53**, 105–116.
25 W. Dong, T. Baird, J. R. Fryer, C. J. Gilmore, D. D. MacNicol, G. Bricogne, D. J. Smith, M. A. O'Keefe and S. Hövmoller, *Nature*, 1992, **355**, 605–609.
26 M. Koshino, H. Kurata and S. Isoda, *Ultramicroscopy*, 2010, **110**, 1465–1474.
27 H. Liu, S. Ryu, Z. Chen, M. L. Steigerwald, C. Nuckolls and L. E. Brus, *J. Am. Chem. Soc.*, 2009, **131**, 17099–17101.
28 J. P. Perdew, K. Burke and M. Ernzerhof, *Phys. Rev. Lett.*, 1997, **78**, 1396–1396.

29 S. Grimme, *J. Comput. Chem.*, 2004, **25**, 1463–1473.

30 S. F. Boys and F. Bernardi, *Mol. Phys.*, 1970, **19**, 553–566.

31 P. A. Redhead, *Vacuum*, 1962, **12**, 203–211.

32 R. Zacharia, H. Ulbricht and T. Hertel, *Phys. Rev. B: Condens. Matter Mater. Phys.*, 2004, **69**, 155406.

33 J. L. Falconer and R. J. Madix, *J. Catal.*, 1977, **48**, 262–268.

34 K. Berland and P. Hyldgaard, *Phys. Rev. B: Condens. Matter*, 2013, **87**, 205421.

35 J. Björk, F. Hanke, C. A. Palma, P. Samori, M. Cecchini and M. Persson, *J. Phys. Chem. Lett.*, 2010, **1**, 3407–3412.

36 D. W. Boukhvalov, M. I. Katsnelson and A. I. Lichtenstein, *Phys. Rev. B: Condens. Matter Mater. Phys.*, 2008, **77**, 035427.

37 Y. Ferro, D. Teillet-Billy, N. Rougeau, V. Sidis, S. Morisset and A. Allouche, *Phys. Rev. B: Condens. Matter Mater. Phys.*, 2008, **78**, 085417.

38 D. W. Boukhvalov and M. I. Katsnelson, *J. Phys.: Condens. Matter*, 2009, **21**, 344205.

39 S. J. Stuart, A. B. Tutein and J. A. Harrison, *J. Chem. Phys.*, 2000, **112**, 6472–6486.

40 G. Algara-Siller, O. Lehtinen, A. Turchanin and U. Kaiser, *Appl. Phys. Lett.*, 2014, **104**, 153115.

41 R. Jones and P. R. Briddon, *Semicond. Semimetals*, 1998, **51**, 287.

42 C. Hartwigsen, S. Goedecker and J. Hutter, *Phys. Rev. B: Condens. Matter*, 1998, **58**, 3641.

43 H. J. Monkhorst and J. D. Pack, *Phys. Rev. B: Solid State*, 1976, **13**, 5188.

44 S. Plimpton, *J. Comput. Phys.*, 1995, **117**, 1–19.

45 C. Koch, Arizona State University, 2002.

46 A. Lubk, F. Röder, T. Niermann, C. Gatel, S. Joulie, F. Houdellier, C. Magén and M. J. Hÿtch, *Ultramicroscopy*, 2012, **115**, 78–87.

47 X. Li, W. Cai, J. An, S. Kim, J. Nah, D. Yang, R. Piner, A. Velamakanni, I. Jung, E. Tutuc, S. K. Banerjee, L. Colombo and R. S. Ruoff, *Science*, 2009, **324**, 1312–1314.

48 M. Woszczyna, A. Winter, M. Grothe, A. Willunat, S. Wundrack, R. Stosch, T. Weimann, F. Ahlers and A. Turchanin, *Adv. Mater.*, 2014, **26**, 4831–4837.